



This is a repository copy of *Combined porogen leaching and emulsion templating to produce bone tissue engineering scaffolds.*

White Rose Research Online URL for this paper:
<http://eprints.whiterose.ac.uk/160991/>

Version: Published Version

Article:

Owen, R., Sherborne, C., Evans, R. et al. (2 more authors) (2020) Combined porogen leaching and emulsion templating to produce bone tissue engineering scaffolds. *International Journal of Bioprinting*, 6 (2). 265. pp. 99-113. ISSN 2424-7723

10.18063/ijb.v6i2.265

Reuse

This article is distributed under the terms of the Creative Commons Attribution-NonCommercial (CC BY-NC) licence. This licence allows you to remix, tweak, and build upon this work non-commercially, and any new works must also acknowledge the authors and be non-commercial. You don't have to license any derivative works on the same terms. More information and the full terms of the licence here:
<https://creativecommons.org/licenses/>

Takedown

If you consider content in White Rose Research Online to be in breach of UK law, please notify us by emailing eprints@whiterose.ac.uk including the URL of the record and the reason for the withdrawal request.



eprints@whiterose.ac.uk
<https://eprints.whiterose.ac.uk/>

Combined Porogen Leaching and Emulsion Templating to produce Bone Tissue Engineering Scaffolds

Robert Owen^{1,2,3}, Colin Sherborne², Richard Evans⁴, Gwendolen C. Reilly^{1,2}, Frederik Claeysens^{1,2*}

¹Department of Materials Science and Engineering, INSIGNEO Institute for in silico Medicine, University of Sheffield, UK

²Department of Materials Science and Engineering, The Kroto Research Institute, University of Sheffield, UK

³Regenerative Medicine and Cellular Therapies, School of Pharmacy, University of Nottingham Biodiscovery Institute, University Park, UK

⁴Bioengineering, Interdisciplinary Programmes Engineering, University of Sheffield, UK

Abstract: Bone has a hierarchy of porosity that is often overlooked when creating tissue engineering scaffolds where pore sizes are typically confined to a single order of magnitude. High internal phase emulsion (HIPE) templating produces polymerized HIPEs (polyHIPEs): highly interconnected porous polymers which have two length scales of porosity covering the 1–100 μm range. However, additional larger scales of porosity cannot be introduced in the standard emulsion formulation. Researchers have previously overcome this by additively manufacturing emulsions; fabricating highly microporous struts into complex macroporous geometries. This is time consuming and expensive; therefore, here we assessed the feasibility of combining porogen leaching with emulsion templating to introduce additional macroporosity. Alginate beads between 275 and 780 μm were incorporated into the emulsion at 0, 50, and 100 wt%. Once polymerized, alginate was dissolved leaving highly porous polyHIPE scaffolds with added macroporosity. The compressive modulus of the scaffolds decreased as alginate porogen content increased. Cellular performance was assessed using MLO-A5 post-osteoblasts. Seeding efficiency was significantly higher and mineralized matrix deposition was more uniformly deposited throughout porogen leached scaffolds compared to plain polyHIPEs. Deep cell infiltration only occurred in porogen leached scaffolds as detected by histology and lightsheet microscopy. This study reveals a quick, low cost and simple method of producing multiscale porosity scaffolds for tissue engineering.

Keywords: Polymerized high internal phase emulsions, Emulsion templating, Alginate, Multiscale porosity, Bone tissue engineering

*Corresponding Author: Frederik Claeysens, Department of Materials Science and Engineering, The Kroto Research Institute, University of Sheffield, UK; f.claeyssens@sheffield.ac.uk

Received: March 06, 2020; **Accepted:** April 01, 2020; **Published Online:** April 30, 2020

Citation: Owen R, Sherborne C, Evans R, *et al.*, 2020, Combined Porogen Leaching and Emulsion Templating of Bone Tissue Engineering Scaffolds, *Int J Bioprint*, 6(2):265. DOI: org/10.18063/ijb.v6i2.265

1 Introduction

Native bone has a hierarchical structure with a range of pore sizes that span multiple length scales^[1]. Inclusion of this multiscale porosity when producing bone tissue engineering scaffolds is often overlooked with pore sizes typically confined to a single order of magnitude. However, it has been demonstrated that a multiscale porosity enhances *in vitro* and *in vivo* performance of scaffolds^[2-4]. The reason for this is that different

size pores promote different functions. Smaller, well interconnected cell-scale porosities promote cell proliferation, migration, and nutrient diffusion, while pore sizes of at least 50 μm but ideally >300 μm have been reported as beneficial for osseous tissue deposition^[5-7].

Polymerized high internal phase emulsions (polyHIPEs) are highly porous materials well suited for three-dimensional (3D) cell culture and tissue engineering, and classically have porosity at

two length-scales: a larger bulk porosity typically in the region of 30 – 50 μm which is interconnected by smaller (1 – 5 μm) pores^[8-18]. As the name suggests, polyHIPE scaffolds are initially formulated as an emulsion. These are typically created by mixing a hydrophobic monomer, crosslinker, initiator, and a suitable surfactant to form the continuous phase of the emulsion, then slowly adding an aqueous internal phase. This creates a water-in-oil (W/O) emulsion where the constant mixing breaks the water into isolated droplets dispersed throughout the continuous monomer phase. To form a high internal phase emulsion (HIPE), the internal phase volume ratio must exceed 74% of the total emulsion as this ensures that droplets form interconnects when polymerized. The continuous phase can be polymerized using either ultraviolet (UV) light or thermal curing; afterward the internal phase drains away leaving behind a highly porous polyHIPE^[19].

The parameters used during the emulsification process directly affect the structure of the final polyHIPE material. Physical actions such as the speed of mixing^[20,21], the rate at which water is added^[22] and the emulsion temperature^[23] all affect internal phase dispersion, geometry, and the final porosity as the droplets act as a template for the continuous phase to polymerize around. Furthermore, the type and quantity of the emulsion constituents also affect the final architecture, including the internal phase volume^[24], monomer type^[25,26], solvent addition^[17], concentration of the surfactant (or particles in Pickering emulsions)^[21,27], initiator solubility^[28], and the concentration of electrolytes in the aqueous phase^[26]. All these affect porosity and/or pore interconnectivity of the polyHIPE. The commercial success of Alvetex[®], a polystyrene polyHIPE, shows the suitability of this class of materials for 3D cell culture^[29]. However, these membranes are only 200 μm thick as cellular penetration into the bulk material is limited, primarily because of factors such as diminishing mass transport and nutrient availability. Furthermore, with polyHIPE scaffolds created from hydrophobic monomers, surface treatments such as plasma etching/coating are necessary to overcome the inherent hydrophobicity of the material. This reduces maximum scaffold

thickness as these treatment methods have limited depth penetration into the material^[30].

These limitations can be overcome by introducing another tier of porosity into the polyHIPE network in the form of larger (>200 μm) pores^[8]. This creates a multiscale porosity scaffold ideal for bone tissue engineering with pore sizes over three length-scales: pore interconnects, standard polyHIPE pores, and additional macropores. Approaches to creating larger pores inherent in the polyHIPE have focused on creating large water droplets in the initial emulsion. This can be done using high temperatures or solvents to destabilize the emulsion in a controlled way to cause droplets of water to coalesce into larger ones^[23]. However, as these changes affect the entire HIPE and larger droplets are formed *in lieu* of smaller ones, this means that a further scale of porosity is not added. Another limitation to this approach is the effect on pore interconnectivity. Pore interconnects form during polymerization between adjacent water droplets if the film of continuous phase surrounding the droplets is sufficiently thin. Below this threshold, the contraction of the material as it polymerizes causes small interconnecting pores to form^[31]; hence, monomers that have high shrinkage during polymerization create more interconnectivity in the polyHIPE scaffold^[25]. Larger water droplets have a thicker continuous phase film surrounding them which will be more resistant to these contraction forces, resulting in fewer interconnects.

An alternative approach to introduce an additional, larger scale of porosity to the polyHIPEs is by 3D printing the HIPE in additive manufacture. By building structures from polyHIPE struts that do not exceed the inherent depth limitations of traditionally manufactured polyHIPEs, porous scaffolds capable of filling larger defects can be produced^[8]. This approach results in multiscale, hierarchical, and interconnected porous scaffolds that have superior nutrient and waste transport while benefiting tissue regeneration. They have smaller (1 – 50 μm) microscale pores that benefit cellular performance and larger pores (>300 μm) that facilitate ingrowth and permit large quantities of extracellular matrix

deposition and vascularization^[32]. PolyHIPE-based additive manufacturing techniques by which this is achievable include emulsion extrusion^[33,34] and microstereolithography-based approaches^[8,9,13,35,36]. The latter has the ability to rapidly polymerize the emulsions and, as we demonstrated recently, inclusion of light-absorbers can afford tight control over the final architecture^[8-10,13].

However, 3D printing emulsions using additive manufacturing technologies require expensive equipment and the trade-off for such architectural fidelity is manufacture speed^[9]. In applications where high levels of control over architecture are essential, such as investigations into the effects of geometry or the production of patient-specific scaffolds^[37], clearly the slower speed of production is worthwhile. Nevertheless, for more generic 3D cell culture applications using stereolithography can have high initial setup costs and be time intensive^[38,39]. Therefore, identifying a simpler approach to introducing a multiscale porosity is warranted. One potential avenue is particulate leaching.

Solvent casting/particulate leaching is a conventional approach to creating scaffold porosity. This process involves dissolving a polymer in a solvent such as dimethylformamide or chloroform then casting around a porogen such as crystals of sugar or salt^[40-42]. These types of porogen are readily available, cheap, and insoluble in hydrophobic solvents. However, this technique can cause limited pore interconnectivity as there is not sufficient contact between the porogens to have a continuous porosity, resulting in “skin” forming around the pores during solvent evaporation. This results in samples often having to be thin to ensure even porogen dispersal and removal^[43,44]. This limitation is alleviated when casting a HIPE around a porogen as the water droplets are deformable ensuring close contact with the porogen. Providing that the porogen material facilitates an open surface porosity, interconnectivity between the emulsion and the voids left by the porogen can be achieved^[19]. As sugar and salt are water-soluble, they are unsuitable porogens for polyHIPEs as they would dissolve in the aqueous

internal phase. Therefore, it is essential to identify a porogen that is insoluble in both emulsion phases whilst giving an open surface porosity. We hypothesize that one such material is alginate, a naturally derived polysaccharide commonly used in tissue engineering due to its biocompatibility, biodegradability, and abundant availability^[45]. By incorporating alginate beads into the HIPE, then polymerizing and subsequently dissolving the alginate, an additional, larger scale of porosity can be quickly, easily and cheaply introduced to the polyHIPE-based scaffolds.

To test this hypothesis, we blended HIPEs with alginate beads at either 50 or 100 wt% of the initial emulsion volume to create polyHIPE scaffolds with a multiscale porosity ranging from 1 to 1000 μm . These were compared to standard polyHIPE materials with a hierarchy of porosity ranging from 1 to 100 μm . To evaluate their performance, MLO-A5 murine post-osteoblasts were cultured for 14 days, with cell proliferation and bone-like matrix deposition by histology and lightsheet microscopy assessed.

2 Materials and methods

Unless otherwise stated, all materials were sourced from Sigma-Aldrich, UK.

2.1 Alginate bead synthesis

Sodium alginate was dissolved in deionized water (diH_2O) at 3 wt% while being mixed (350 rpm) on a magnetic stirrer hot-plate maintained at 30°C. To create the beads, this solution was loaded into a 3 mL fluid dispensing barrel (Nordson EFD), sealed using a dispensing piston (InterTronic), and injected through a 30 gauge tip (internal diameter 0.15 mm, Nordson EFD) from a height of 100 mm into a cross-linking solution of calcium chloride (20 wt% in diH_2O) using a mechanical syringe pump (Ultra 2800 Positive Displacement Dispenser, Nordson EFD) at 0.2195 mL/s. Beads below 710 μm were selectively collected through sieving and stored in diH_2O until needed. To assess size distribution, 50 images were taken of bead populations (Motic Images Plus software) and diameters measured using Fiji^[46,47].

2.2 PolyHIPE synthesis

For the continuous phase of the emulsion, the monomer 2-ethylhexyl acrylate (26 g) was mixed with the crosslinker trimethylolpropane triacrylate (7 g). The surfactant Hypermer B246-SO-(MV) was added at 10 wt% (3.3 g) relative to the total weight of the acrylates (33 g) and mixed until dissolved. To create the emulsion, 2 g of this stock solution was taken and a photoinitiator (diphenyl (2,4,6-trimethylbenzoyl) phosphine oxide/2-hydroxy-2-methylpropiophenone) was added at 5 wt% (0.1 g). This solution was continuously mixed at 350 rpm using a paddle stirrer (Pro40 scientific stirrer, SciQuip). While mixing, diH₂O (diH₂O, 18 mL) was added dropwise to form a 90 vol% W/O HIPE. Where alginate beads were incorporated, beads were patted dry and weighed, then either 50 or 100 wt% relative to the total amount of emulsion was added to the HIPE (e.g. 100 wt% means 4 g of beads were added to 4 g of HIPE). The blend was then stirred for a further 2 min at 350 rpm to homogenize the beads. Herein, these three compositions will be referred to as “plain,” “50 wt%,” and “100 wt%” polyHIPEs. This refers to the content of the alginate bead porogen in the HIPE.

To polymerize the emulsion, it was poured into a square, PTFE mold with a glass base and top

(45 × 45 × 6.2 mm), filled with approximately 12.5 mL of HIPE and placed under 100 W UV light (Omnicure S1500 with adjustable spot collimating adaptor, Excelitas Technologies), for 180 s on both sides. With these dimensions and exposure times the polyHIPEs were fully cured with no cavity left in the center of the monolith. The polyHIPEs were removed from the mold and washed in acetone to remove any uncured monomer. To remove the alginate, polyHIPEs were soaked in 0.2 M sodium citrate in diH₂O for 2 h with sonication. The samples were then dried overnight under vacuum. A schematic of the fabrication process is given in **Figure 1**. To produce cubes for cell culture the outer surfaces, including the top surface and polymer skin on the glass cured sides, were removed using a scalpel. The remaining bulk polyHIPE was then cut into 5 × 5 × 5 mm cubes.

To produce cylinders for mechanical testing, the HIPE was polymerized in a 3 mL syringe (internal diameter 8.2 mm). The cylinders were washed using the same methods described above and then cut into 10 mm lengths. The surface skin surrounding the outside of these cylinders was retained to keep a constant volume of material.

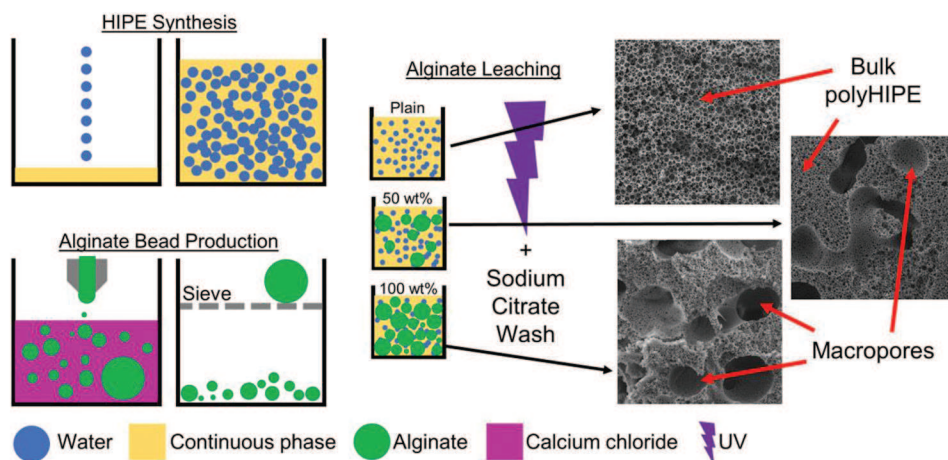


Figure 1. Schematic detailing the alginate-leached polymerized high internal phase emulsions synthesis. A 90% internal phase volume HIPE is synthesized by adding water to the continuous phase. Alginate beads are produced by injecting an alginate solution to calcium chloride and sieving. Alginate beads are then mixed into HIPEs at either 0, 50 or 100 wt% of the HIPE. Emulsions are then UV polymerized, washed in acetone and the alginate dissolved using sodium citrate. Macropores within the bulk of the polyHIPE left by alginate beads are clearly visible in the 50 and 100 wt% scaffolds.

2.3 Scanning electron microscopy (SEM)

Samples were sputter coated with gold (SC500, Emscope) to improve conductivity before imaging (XL-20 SEM, Philips).

2.4 Mechanical testing

Compressive testing was performed on a BOSE ElectroForce 3200 with a 450 N load cell at a rate of 0.01 mm/s to a maximum displacement of 4 mm. The samples were placed centrally on parallel compression plates and a preload of 1 N applied before test initiation. The compressive modulus was calculated from the force-displacement curves.

2.5 Plasma modification

To increase hydrophilicity for cell culture, polyHIPE samples were air plasma treated (Zepto W6 Plasma System, Diener Electronic). The samples were placed uniformly on a flat aluminum foil wrapped stage and placed centrally in the plasma chamber. A range of parameters were tested as charring readily occurred in the particulate leached polyHIPEs. The final parameters used were 15 W at an initial pressure of 0.4 mbar for 1 min.

2.6 Cell culture

MLO-A5 murine post-osteoblasts (kindly donated by Dr. Lynda Bonewald, University of Missouri) were used for all experiments. Cells were passaged in gelatin-coated flasks in basal media (BM) consisting of alpha-minimum essential medium (alpha-MEM) (Lonza, UK) with 10% fetal bovine serum (FBS, Labtech, UK), 2 mM L-glutamine, 100 U/mL penicillin, and 100 µg/mL streptomycin.

To sterilize, scaffolds were placed in 70% ethanol and put under vacuum to remove all air. After 90 min, ethanol was exchanged for phosphate-buffered saline (PBS) and orbitally shaken at 150 rpm for 15 min. The washing stage was repeated a further 2 times, then PBS was exchanged for BM for 1 h. Media were removed from the scaffolds for seeding.

To seed, scaffolds were placed in a 96 well plate. 350,000 MLO-A5 in 100 µL BM were

added to the well, just covering the top scaffold surface. The seeding suspension was gently pulsed by manual pipetting every 45 min to improve seeding distribution. After 2 h, scaffolds were transferred to a 48 well plate so that only adhered cells remained. Cell viability (PrestoBlue) was quantified to determine baseline cell numbers, then scaffolds were maintained in supplemented media (SM) consisting of BM with 5 mM beta-glycerolphosphate and 50 µg/mL ascorbic acid 2-phosphate. Media were changed every 2–3 days.

2.7 Cell viability

Viability was quantified on days 0, 7, and 14 by PrestoBlue which measures metabolic activity. PrestoBlue reagent was diluted 1:10 in Hank's Balanced Salt Solution. 1 mL was added to each well and incubated for 1 h. 200 µL of the reduced solution was then transferred in triplicate to a black 96 well plate and the fluorescence measured on a plate reader (Tecan infinite 200-pro, λ_{ex} 540 nm, λ_{em} 590 nm). Scaffolds were rinsed in PBS before adding fresh SM.

2.8 Mineralized matrix deposition

Calcium and collagen deposition were quantified on days 7 and 14 by alizarin red S (ARS) and direct red 80 (DR80), respectively, as previously reported Owen *et al.*^[48] Briefly, the samples were rinsed twice in PBS then fixed by immersion in 3.7% formaldehyde for 30 min. Scaffolds were rinsed twice in diH₂O, and then submerged in 1 w/v% ARS in diH₂O for 30 min to stain for calcium. Stained samples were washed repeatedly in diH₂O until wash water remained clear, then air dried and photographed. To quantify, scaffolds were submerged in 1 mL 5% perchloric acid and orbitally shaken for 15 min at 100 rpm. 150 µL was then transferred in triplicate to a 96 well plate and read at an absorbance of 405 nm (Tecan infinite 200-pro). The concentration of ARS was determined from a standard curve. Scaffolds were then washed 3 times in diH₂O before immersing in 1 w/v% DR80 in saturated picric acid for 1 h to stain for collagen. Stained samples were washed repeatedly in diH₂O until wash water

remained clear, then air dried and photographed. To quantify, scaffolds were submerged in 1 mL of 0.2 M sodium hydroxide; methanol and orbitally shaken for 15 min at 100 rpm. 150 μ L was then transferred in triplicate to a 96 well plate and read at an absorbance of 540 nm (Tecan infinite 200-pro). The concentration of DR80 was determined from a standard curve.

2.9 Histology

Scaffold infiltration was assessed on days 7 and 14 by histology. Scaffolds were fixed as above before being submerged in optimal cutting temperature medium (Leica) and placed under vacuum for 1 h then snap-frozen in liquid nitrogen. Sections were obtained using a cryostat (Leica CM1860 UV) at -24°C at 10 μ m thickness, mounted onto a glass slide and stained with hematoxylin and eosin. After staining, the samples were preserved under a cover glass and imaged under a Motic microscope using a digital camera.

2.10 Lightsheet microscopy

As a further measure of cell ingress, live/dead staining was performed on day 14 and assessed by lightsheet microscopy. Scaffolds were rinsed in PBS then stained in 2 μ M calcein AM (live cells) in PBS for 30 min at room temperature. Scaffolds were then rinsed in PBS, submerged in 20 μ g/mL propidium iodide (dead cells) in alpha-MEM for 5 min at room temperature, then rinsed twice in PBS. Scaffolds were then cut using a scalpel (one vertical and one horizontal) so that internal surfaces could be imaged to assess ingrowth.

To image through lightsheet microscopy (Z.1 lightsheet microscope, Zeiss), scaffold sections were mounted in 0.8 vol% agarose in diH₂O in glass capillaries (size 4, Zeiss). Two 10 \times NA 0.2 illumination optics (Zeiss) were used to illuminate the samples in combination with a W plan-apochromat 20 \times /1.0 objective (Zeiss). The samples were excited using a 405 nm (20 mW) and a 488 nm (50 mW) laser. Z-stacks were taken and a maximum projection image created using the Bio-Formats plug-in for Fiji^[49].

2.11 Statistical analysis

All statistical analysis was performed in GraphPad Prism (version 7.00). Data presented as mean \pm standard deviation. Compressive moduli were compared by one-way analysis of variance (ANOVA) with Tukey's post-test. Cell culture results were compared by two-way ANOVA with Tukey's post-test. Mineral and collagen quantification are normalized to the "plain polyHIPE" at each time point. The differences were considered significant when $P < 0.05$ (*) and are indicated on the figures and in the legend. All cell culture experiments were repeated twice in triplicate.

3 Results

3.1 Alginate porogen leaching within polyHIPEs creates multiscale porosity

Alginate beads were created by injecting the alginate solution through a 30 G needle into 0.2 M calcium chloride solution at 0.2195 mL/s before passing through a 710 μ m sieve. The size distribution of sieved alginate beads fitted a Gaussian distribution with diameters ranging from 275 μ m to 780 μ m, with a modal range bead size of 500-550 μ m and a mean diameter was 532 μ m (**Figure 2A**). A small number of beads exceeded the 710 μ m sieve mesh size due to bead deformation during sieving. There was no further sieving or intentional separation of the alginate beads into different sizes.

A polyHIPE with multiscale porosity was created when alginate beads were mixed into the HIPE before polymerization. SEM images of plain (0 wt%, **Figure 2B and C**), 50 wt% (**Figure 2D and E**), and 100 wt% (**Figure 2F and G**) polyHIPEs reveal the macroporosity present in the material when alginate beads were incorporated. Pore sizes ranged from \sim 1 to 10 μ m for the polyHIPE pore interconnects, \sim 10 to 50 μ m for the polyHIPE emulsion pores, and up to \sim 780 μ m for the alginate bead porogen pores. At 100 wt%, macropores formed by alginate-leaching frequently interconnected, leaving large channels throughout the scaffold. The polymer struts at the interface of the bulk polyHIPE porosity and the pores formed

by the alginate beads are smooth and form an open porosity with a similar morphology to the polyHIPE surface that cures against air on the top of the emulsion.

3.2 Porogen leaching of polyHIPEs decreases the compressive modulus

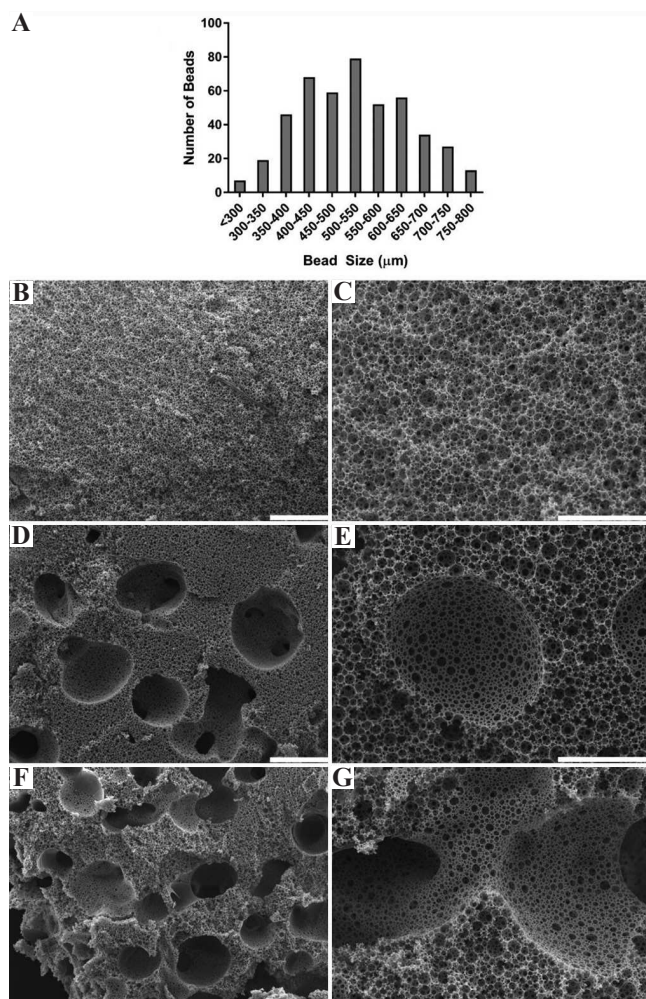


Figure 2. (A) Alginate bead size distribution after sieving. Low (B, D, F, scale bars 500 μm) and high (C, E, G, scale bars 200 μm) magnification scanning electron microscopy images of (B and C) plain polymerized high internal phase emulsions (polyHIPEs), (D and E) 50 wt% alginate bead polyHIPEs, and (F and G) 100 wt% alginate bead polyHIPEs. Large macropores left by alginate beads clearly visible in the 50 and 100 wt% polyHIPEs (D-G), with interconnection between macro pores occurring at the highest wt% (G).

The compressive modulus of the polyHIPE decreased as alginate bead content increased (**Figure 3**). A linear relationship was observed between wt% of alginate beads and compressive moduli ($R^2 = 0.998$).

3.3 Porogen leached polyHIPE had superior mineralized matrix distribution

Seeding efficiency was significantly higher on the 100 wt% alginate porogen leached polyHIPE scaffolds in comparison to plain scaffolds, with approximately 30% higher metabolic activity observed on day 0 ($P < 0.05$, **Figure 4A**). By day 14, metabolic activity was still significantly higher (100 wt% vs. plain, $P < 0.05$). Calcium deposition by ARS staining was greatest on the plain scaffold in comparison to both porogen leached scaffolds on day 7 ($P < 0.05$), but there was no significant difference by day 14 (**Figure 4B**). Collagen deposition by DR80 staining on the 50 wt% polyHIPEs was significantly lower on day 7 in comparison to 100 wt% polyHIPEs ($P < 0.05$), with no significant differences between any group

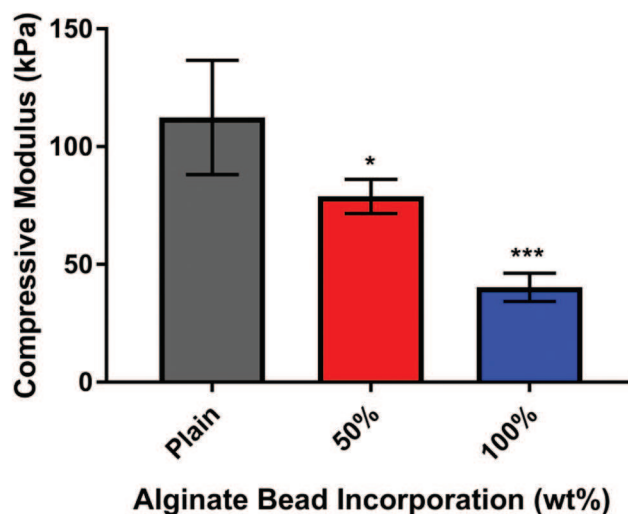


Figure 3. Compressive modulus of polymerized high internal phase emulsions (polyHIPEs) at different alginate bead incorporation. Porogen leaching with alginate significantly reduced the compressive moduli at 50 wt% ($P < 0.05$) and 100 wt% ($P < 0.001$) in comparison to plain polyHIPEs ($n = 4$).

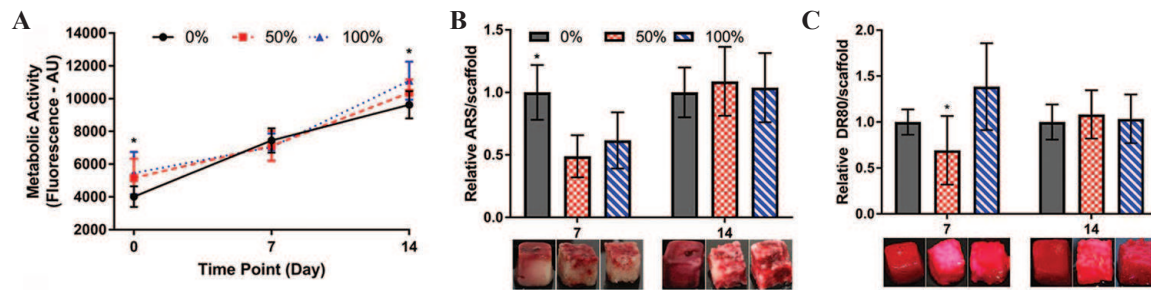


Figure 4. Cell growth and mineralized matrix deposition on polymerized high internal phase emulsions (polyHIPE) scaffolds. (A) Metabolic activity over 14 days, 100 wt% significantly higher than plain on day 0 and 14 ($P < 0.05$). (B) Calcium deposition on days 7 and 14. Typical mineral staining for each condition shown immediately below each bar. Plain significantly higher than 50 wt% and 100 wt% on day 7 ($P < 0.05$), no significant differences by day 14. (C) Collagen deposition on days 7 and 14. Typical collagen staining for each condition showed immediately below each bar. 50 wt% had significantly less collagen than 100 wt% on day 7 ($P < 0.05$), no significant differences by day 14. Matrix staining is confined to the outer surfaces on plain polyHIPEs at both time points, whereas in alginate-leached polyHIPEs, penetration into the bulk of the material is visible.

by day 14. For plain scaffolds, both ARS and DR80 staining remained confined to the exterior scaffold surfaces at both time points. However, on alginate-leached scaffolds, positive staining was observed deeper within the bulk of the material.

3.4 Cell ingrowth is superior in porogen leached polyHIPE scaffolds

In porogen leached scaffolds, cell infiltration is visible much further into the scaffold, with the greatest ingrowth observed in the 100 wt% scaffolds (Figure 5). In plain scaffold cells are constrained to the exterior surface and first 2 – 3 rows of polyHIPE pores, achieving a maximum infiltration distance of approximately 50 μm . In contrast, in the 50 wt% scaffolds cellular penetration had reached a depth of approximately 200 μm by day 7 and up to 450 μm by day 14. For the 100 wt% scaffolds, infiltration depths over 600 μm from the outer surface were observed at both time points.

3.5 Cells remain viable within the center of the porogen leached polyHIPE scaffolds

Live/dead staining assessed by lightsheet microscopy was performed on day 14. After staining, the samples were cut horizontally and vertically and placed into the lightsheet microscope

to image the internal surfaces of the samples and assess cell ingrowth. The external seeding surface is on the right side of each image.

On the plain scaffold, cells were confined to the scaffold surface, with no cell ingrowth past the first layers of pores (Figure 6A). In the 50 wt% porogen leached scaffold, viable cells were visible over the internal network of the scaffold, although a higher concentration of dead cells was present further into the structure (Figure 6B). For the 100 wt% scaffold identifying the edge of the scaffold was more difficult, as there was no clear linear region due to the high macroporosity. The cells were visible deep into the scaffold internal network and were predominately viable (green) cells (Figure 6C). Due to the autofluorescence of the polyHIPE material, there is a weak green signal throughout the imaging.

4 Discussion

In this study, we combined alginate bead porogen leaching with emulsion templating to introduce an additional, larger length-scale of porosity to polyHIPEs, creating a multiscale porosity over three length-scales. To the best of our knowledge, this is the first-time such multiscale porous polyHIPEs have been fabricated using a single-step alginate porogen leaching approach.

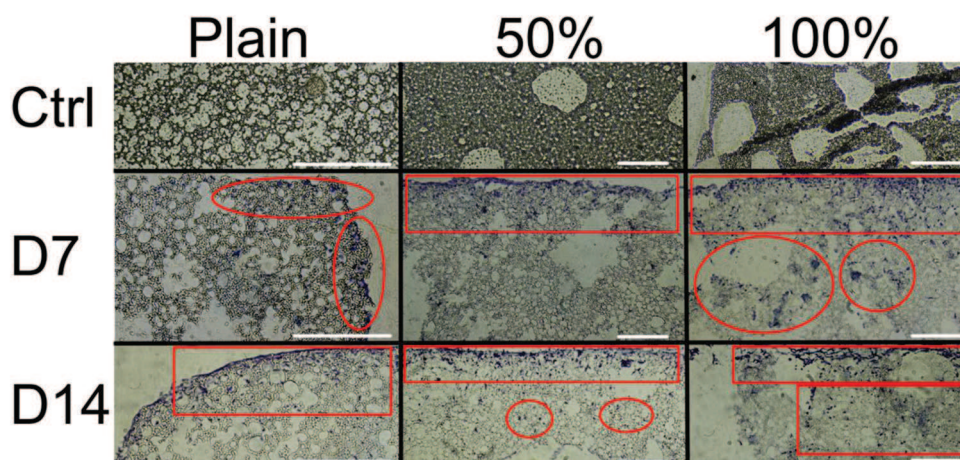


Figure 5. Representative histological sections of plain, 50 wt% and 100 wt% polymerized high internal phase emulsions scaffolds. (Top row) control, cell free sections (Middle and bottom rows) day 7 and 14 ingrowth, respectively. Ingrowth is highlighted in red circled regions. Cells are confined to the top surface in plain scaffolds, whereas infiltration through the material is present in alginate leached scaffolds. The greatest infiltration occurs in the 100 wt% scaffolds. Scale bars 200 μm .

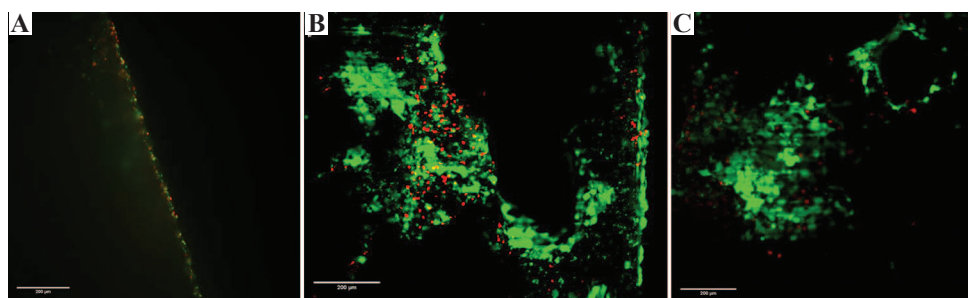


Figure 6. Representative lightsheet microscopy of live (green)/dead (red) staining on polymerized high internal phase emulsions (polyHIPE) scaffolds. Right side of the images is the external surface, further left is deeper into the material. The polyHIPE material auto-fluoresces in the green wavelength. (A) Plain scaffolds – cells were confined to the scaffold surface (B and C) 50 and 100 wt%, respectively – cell ingrowth occurs deep into the material with a lower observed number of dead cells in the 100 wt% composition Scale bars 200 μm .

The effect of porosity on the culture of MLO-A5 post-osteoblast cells was studied, highlighting the potential of this scaffold manufacturing method for bone tissue engineering related applications. We propose alginate porogen leaching as a cheap and simple method to produce additional larger pores within the polyHIPE scaffolds.

We envisage that these porous materials will be useful as 3D substrates for bioprinting. They will allow complex tissues to be engineered that include multiple cell types by combining these new materials with the spatially controlled deposition of cells through bioprinting. In addition, there is

an emergent research field exploring formulations of HIPEs that are compatible with bioprinting^[34] and this combination will, in our viewpoint, lead to a powerful new hybrid technology to build 3D organs.

To the best of our knowledge, only one previous study has investigated combining particulate leaching with emulsion templating of materials. This approach first sintered poly(methyl methacrylate) (PMMA) beads for 24 h to fuse them together to create a sacrificial mold, then HIPE was poured over these sintered beads and polymerized. Subsequently, the PMMA was dissolved by

ethyl acetate leaving a polyHIPE with $\sim 100 \mu\text{m}$ macropores from the PMMA beads^[50]. While this approach successfully generated multiscale porosity polyHIPEs, it is complex and time consuming. This is due to the extended sintering time and the use of Soxhlet washing to remove the PMMA and residual solvent; both essential steps to form the macropores and minimize cytotoxicity. Furthermore, the $100 \mu\text{m}$ macropores introduced here are still a limiting factor as vascularization requires larger macropores^[6]. In addition, as cellular penetration also depends on pore size and monolith thickness^[51,52], ingrowth can be further improved by introducing larger macropores as shown here. Importantly, our findings showing that an increased macroporosity increases cell infiltration agree with those of Paljevac *et al.*, which demonstrates its value in tissue engineering and 3D cell culture^[50].

Alternative work within our group has focused on using stereolithography to introduce this larger length-scale hierarchical porosity into polyHIPEs^[8-11,13], and various alternative additive manufacturing techniques have also been used by other groups^[33,35]. While these approaches produce structures with well-defined architectures; they are not without their limitations. Laser-based systems are expensive to set up and control over the final structure requires time-consuming process optimization. Furthermore, the emulsions scatter light; therefore, for high resolution 3D printing the addition of light-absorbers is needed to control the polymerized region^[9]. Therefore, in applications where a multiscale porosity is beneficial, but the final scaffold architecture does not have to be precisely defined, for example, initial 3D cell culture investigations, a more straightforward approach, such as porogen leaching may be desirable.

In emulsion templating, the internal phase acts as a template for the continuous phase to polymerize around. This is like porogen leaching in that the monomer is polymerized around something immiscible with it. The size of the water droplets directly affects the pore size, as does the size of the sugar/salt crystals in porogen leaching. The benefit of using a liquid porogen

rather than crystals is that it can be deformed to accommodate a high packing efficiency yielding a much higher porosity. At high water volume ratios ($>74\%$), droplets are forced to deform and become polygonal but remain separated by a thin layer of the monomer/surfactant solution. This thin monomer film is a precursor for interconnectivity as the monomer contracts during polymerization to create interconnecting holes between adjacent pores^[31]. However, creating numerous large pores ($>200 \mu\text{m}$) solely by tailoring the emulsion conditions to have large water droplets will often result in limited pore interconnectivity. This is because the large water droplets are surrounded by a thick monomer film that resists the contraction forces that create interconnectivity during polymerization. On the other hand, smaller droplets of water have a higher surface area, so the monomer layer surrounding it will be thinner and more prone to the contraction forces that create the interconnectivity^[25]. As shown here, the addition of a non-emulsion-based method is ideal for creating large pores independent of the emulsion conditions.

Alginate beads with a size distribution between 275 and $780 \mu\text{m}$ were made by injecting an alginate solution into a calcium chloride solution. The size distribution of the alginate beads represents the range that could be produced when using the fastest injection speed on the mechanical syringe pump and forcing the alginate solution through a 30 G needle. Some of the alginate beads had a slight non-spherical shape, which is most likely because of a combination of high injection speed, the viscosity of the injected alginate solution not having enough time in flight to form a sphere, and the fast gelation of these beads as they hit the calcium chloride solution. It required the maximum injection speed of the pump (0.2195 mL/s through a 3 mL syringe) and small needle size to extrude the viscous alginate solution fast enough to produce the smallest droplets. However, this occasionally caused some alginate solution to leak past the syringe's internal plastic seal during the injection process. In turn, this would reduce the internal syringe pressure and therefore the speed at which the alginate solution was being injected

into the calcium chloride solution, thus forming larger beads.

In initial experiments (data not shown), we produced very large millimeter-sized beads when a slower speed or larger gauge needle was used. Furthermore, very large beads were often created when setting up and removing the syringe as the alginate solution could occasionally drop into the calcium chloride solution; hence, all alginate beads above 780 μm were sieved out after bead manufacture was complete. The alginate beads were not sieved further, as we wanted to preserve the size distribution to create a range of macropores within the polyHIPE; a polydisperse bead distribution should have a better packing efficiency than a monodisperse one yielding an interconnected macropore network throughout the scaffold. However, alternative direct fabrication methods to have tighter control over alginate bead size and shape may be desirable. These could include electrospraying^[53] and microfluidics^[54] to produce a more monodisperse size distribution.

The ratios of alginate beads (0, 50, and 100 wt%) relative to the initial HIPE weight were chosen as this broad range affords us a baseline understanding of the feasibility of combining alginate bead porogen leaching with emulsion templating and their effect on the polyHIPE scaffold morphology. Here, alginate beads were incorporated into the HIPE at up to 100 wt% of the emulsion with no visual signs of emulsion destabilization. The polymer struts of the polyHIPE surface that has cured against the alginate beads have a smooth surface composed of numerous pores of different sizes. Rather than the classical polyHIPE morphology observed in the bulk of the plain polyHIPE, the pore shape at this interface appears different as the water droplets in the initial emulsion have been pressed and deformed against the smooth alginate surface before polymerization. Regardless of the shape of the alginate bead the polyHIPE retained an open pore surface and overall mirrored the curved shape of the alginate it cured against. The polymerized boundary layer between the alginate surface and polyHIPE had open connected pores. We assume this is because the alginate beads are 97% water

and therefore will have a thin layer of water surrounding them. This means that the emulsion interface around these large alginate beads should be the same as if it were a water droplet – it will be surrounded by a thin film of surfactant stabilized monomer that on polymerization would contract to create an open surface porosity. As the alginate beads have been made in a separate process to the emulsion, both the porosity in the polyHIPE from the water droplets and the macropores from the alginate beads can be controlled independently to each other, unlike when heating or solvent destabilization is used^[23].

As expected, when porosity increased compressive modulus decreased (**Figure 3**). Interestingly, as porosity increased the standard plasma treatment applied to polyHIPEs to increase hydrophilicity in our group resulted in sample charring (data not shown)^[17]. We hypothesize that this is due to the high energy ions in the plasma impacting and accumulating within the polyHIPE macropores introduced by alginate bead leaching, resulting in localized heating and charring. This is supported by greater charring occurring in the 100 wt% than the 50 wt% alginate porogen leached polyHIPE scaffolds, and the apparent localization of the charring to the macropores. In the plain polyHIPEs which do not possess these macropores, these ions are carried over the surface of the polyHIPE meaning that no charring occurs. To alleviate this, the combination of lower power, reduced starting pressure to increase air flow rate, and shorter treatment times were tested, finding that a 70% reduction in power eliminated the charring entirely whilst still reducing the hydrophobicity of the scaffold.

Seeding efficiency was significantly greater in the 100 wt% scaffolds than the plain polyHIPEs as the larger pores allowed cells and media to penetrate the porous network more easily (**Figure 4A**). Although there was no significant difference at day 7, metabolic activity was significantly higher in 100 wt% samples than plain polyHIPEs by day 14. PrestoBlue measures the reduction of resazurin to fluorescent resorufin. This must be completely eluted from the samples for the fluorescence to correlate to the cell number. This is more difficult

in highly porous samples where cells reside deep within the scaffold encased in extracellular matrix than in plain polyHIPE scaffolds where cells are all the outer edges. Therefore, it is likely that cell number could be increasingly underestimated as scaffold porosity increases.

At day 7, mineralized matrix deposition was lower in porogen leached polyHIPEs than plain ones (**Figure 4B and C**). As osteoblasts do not begin to deposit mineralized matrix until confluent^[54], the increased potential for ingrowth into porogen leached samples likely meant that MLO-A5 were still in a proliferative state, at this time point, hence the lower calcium deposition. These differences were no longer present by day 14, which indicate a faster rate of matrix deposition in the porogen leached scaffolds in the 2nd week than the plain. Furthermore, a similar quantity of mineralized matrix was deposited in the alginate-leached scaffolds to the plain scaffolds by day 14 despite having a significantly reduced culture area due to the presence of alginate beads during polymerization (up to 50% less total material in the case of the 100 wt% scaffolds). Considering all scaffolds had the same exterior dimensions ($5 \times 5 \times 5$ mm), this indicates a better distributed neo-tissue formation throughout the alginate leached scaffolds. Photographs of scaffolds before destaining show how mineral distribution was more uniform in the porogen leached scaffolds at both time points, whereas it was confined to the exterior surfaces in plain scaffolds. These observations on matrix distribution from low magnification photographs agree with the histology and lightsheet microscopy (**Figures 5 and 6**). In both techniques, cells and matrix in plain polyHIPEs are only apparent on the outer perimeter of the scaffold. In contrast, infiltration readily occurred on porogen leached scaffolds, with the greatest ingrowth occurring on the most porous scaffolds and viable cells being present in the scaffold millimeter(s) from the outer surface. This deeper infiltration likely occurs for two reasons. First, the connected macroporosity left by the alginate beads provides a facile route for cells to enter the bulk of the scaffold during seeding. Second, improved diffusion throughout the scaffold due to the additional macroporosity

encourages deeper cell penetration into the polyHIPE network as cells have greater nutrient availability and waste transport in comparison to plain scaffolds at these deeper locations.

In summary, we have shown that alginate-bead porogen-leaching of polyHIPEs can be performed in a single-step process. This quickly and easily produces multiscale porosity scaffolds with pore sizes spanning three orders of magnitude (1 – 1000 μ m). This approach enhances initial cell seeding efficiency, promotes ingrowth and uniform matrix deposition, and allows cells to remain viable deep within the scaffold. Overall, these findings have implications in tissue engineering of both bone and other tissues due to the ability to recreate the hierarchical porosities observed in a wide range of natural biological tissues.

Authors' contributions

Conceptualization (RO, GR, FC), data curation (RO), formal analysis (RO, CS, RE), funding acquisition (RO, GR, FC), investigation (RO, CS, RE), methodology (RO, CS, RE), project administration (RO, CS, RE, GR, FC), resources (GR, FC), supervision (RO, CS, GR, FC), validation (RO, CS, RE, GR, FC), visualization (RO), writing – original draft (RO), and writing – review and editing (RO, GR, FC).

Conflicts of interest

The are no conflicts of interest to declare

Acknowledgments

We acknowledge funding from the Engineering and Physical Sciences Research Council (Grant no. EP/L505055/1 and EP/N509735/1) and Biotechnology and Biological Sciences Research Council (Grant no. BB/F016840/1). We also acknowledge the EPSRC Henry Royce Institute funding (Grant No. EP/P02470X/1) for the light sheet microscope.

References

1. Wu S, Liu X, Yeung KW, *et al.*, 2014, Biomimetic Porous Scaffolds for Bone Tissue Engineering. *Materials Sci Eng R*

- Rep*, 80:1–36.
- Gupta D, Singh AK, Dravid A, *et al.*, 2019, Multiscale Porosity in Compressible Cryogenically 3D Printed Gels for Bone Tissue Engineering. *ACS Appl Mater Interfaces*, 11:20437–52. DOI: 10.1021/acsami.9b05460
 - Rustom LE, Boudou T, Nemke BW, *et al.*, 2017, Multiscale Porosity Directs Bone Regeneration in Biphasic Calcium Phosphate Scaffolds. *ACS Biomater Sci Eng*, 3:2768–78. DOI: 10.1021/acsbiomaterials.6b00632
 - Woodard JR, Hilldore AJ, Lan SK, *et al.*, 2007, The Mechanical Properties and Osteoconductivity of Hydroxyapatite Bone Scaffolds with Multi-scale Porosity. *Biomaterials*, 28:45–54. DOI: 10.1016/j.biomaterials.2006.08.021
 - Roosa SM, Kempainen JM, Moffitt EN, *et al.*, 2010, The Pore Size of Polycaprolactone Scaffolds has Limited Influence on Bone Regeneration in an *in vivo* Model. *J Biomed Mater Res A*, 92:359–68. DOI: 10.1002/jbma.a.32381
 - Vand K, Kaplan D, 2005, Porosity of 3D Biomaterial Scaffolds and Osteogenesis. *Biomaterials*, 26:5474–91. DOI: 10.1016/j.biomaterials.2005.02.002
 - Land LQ, Choong C, 2013, Three-dimensional Scaffolds for Tissue Engineering Applications: Role of Porosity and Pore Size. *Tissue Eng Part B Rev*, 19:485–502. DOI: 10.1089/ten.teb.2012.0437
 - Owen R, Sherborne C, Paterson T, *et al.*, 2016, Emulsion Templated Scaffolds with Tunable Mechanical Properties for Bone Tissue Engineering. *J Mech Behav Biomed Mater*, 54:159–72. DOI: 10.1016/j.jmbbm.2015.09.019
 - Sherborne C, Owen R, Reilly GC, *et al.*, 2018, Light-based Additive Manufacturing of PolyHIPEs: Controlling the Surface Porosity for 3D Cell Culture Applications. *Mater Des*, 156:494–503. DOI: 10.1016/j.matdes.2018.06.061
 - Malayeri A, Sherborne C, Paterson T, *et al.*, 2016, Osteosarcoma growth on trabecular bone mimicking structures manufactured via laser direct write. *Int J Bioprint*, 2:67–72. DOI: 10.18063/ijb.2016.02.005
 - Owen R, Sherborne C, Reilly GC, *et al.*, 2015, Data for the Analysis of PolyHIPE Scaffolds with Tunable Mechanical Properties for Bone Tissue Engineering. *Data Brief*, 5:616–20. DOI: 10.1016/j.dib.2015.09.051
 - Paterson TE, Gigliobianco G, Sherborne C, *et al.*, 2018, Porous Microspheres Support Mesenchymal Progenitor Cell Ingrowth and Stimulate Angiogenesis. *APL Bioeng*, 2:026103. DOI: 10.1063/1.5008556
 - Wang AJ, Paterson T, Owen R, *et al.*, 2016, Photocurable High Internal Phase Emulsions (HIPEs) Containing Hydroxyapatite for Additive Manufacture of Tissue Engineering Scaffolds with Multi-scale Porosity. *Mater Sci Eng C*, 67:51–8. DOI: 10.1016/j.msec.2016.04.087
 - Whitely M, Rodriguez-Rivera G, Waldron C, *et al.*, 2019, Porous PolyHIPE Microspheres for Protein Delivery from an Injectable Bone Graft. *Acta Biomater*, 93:169–79. DOI: 10.1016/j.actbio.2019.01.044
 - Lee A, Langford CR, Rodriguez-Lorenzo LM, *et al.*, 2017, Bioceramic Nanocomposite Thiol-acrylate polyHIPE Scaffolds for Enhanced Osteoblastic Cell Culture in 3D. *Biomater Sci*, 5:2035–47. DOI: 10.1039/c7bm00292k
 - Dikici BA, Reilly GC, Claeysens F, 2020, Boosting the Osteogenic and Angiogenic Performance of Multiscale Porous Polycaprolactone Scaffolds by *in vitro* Generated Extracellular Matrix Decoration. *ACS Appl Mater Interfaces*, 12:12510–24. DOI: 10.1021/acsami.9b23100
 - Dikici BA, Sherborne C, Reilly GC, *et al.*, 2019, Emulsion Templated Scaffolds Manufactured from Photocurable Polycaprolactone. *Polymer*, 175:243–54. DOI: 10.1016/j.polymer.2019.05.023
 - Dikici BA, Dikici S, Reilly GC, *et al.*, 2019, A Novel Bilayer Polycaprolactone Membrane for Guided Bone Regeneration: Combining Electrospinning and Emulsion Templating. *Materials (Basel)*, 12:12162643. DOI: 10.3390/ma12162643
 - Cameron NR, 2005, High Internal Phase Emulsion Templating as a Route to Well-defined Porous Polymers. *Polymer*, 46:1439–49. DOI: 10.1016/j.polymer.2004.11.097
 - Krajnc PH, 2014, PolyHIPEs from Methyl Methacrylate: Hierarchically Structured Microcellular Polymers with Exceptional Mechanical Properties. *Polymer*, 55:4420–4. DOI: 10.1016/j.polymer.2014.07.007
 - Iand G, Silverstein MS, 2010, Polymerized pickering HIPEs: Effects of synthesis parameters on porous structure. *J Polym Sci Part A Polym Chem*, 48:1516–25. DOI: 10.1002/pola.23911
 - Bokhari M, Carnachan RJ, Przyborski SA, *et al.*, 2007, Emulsion-templated Porous Polymers as Scaffolds for Three Dimensional Cell Culture: Effect of Synthesis Parameters on Scaffold Formation and Homogeneity. *J Mater Chem*, 17:4088–94. DOI: 10.1039/b707499a
 - Carnachan RJ, Bokhari M, Przyborski SA, *et al.*, 2006, Tailoring the Morphology of Emulsion-templated Porous Polymers. *Soft Matter*, 2:608–16. DOI: 10.1039/b603211g
 - Richez A, Deleuze H, Vedrenne P, *et al.*, 2005, Preparation of Ultra-low-density Microcellular Materials. *J Appl Polym Sci*, 96:2053–63. DOI: 10.1002/app.21668
 - Xu H, Zheng X, Huang Y, *et al.*, 2016, Interconnected Porous Polymers with Tunable Pore Throat Size Prepared via

- Pickering High Internal Phase Emulsions. *Langmuir*, 32:38–45. DOI: 10.1021/acs.langmuir.5b03037
26. Williams JM, Gray AJ, Wilkerson MH, 1990, Emulsion Stability and Rigid Foams from Styrene or Divinylbenzene Water-in-oil Emulsions. *Langmuir*, 6:437–44. DOI: 10.1021/la00092a026
 27. Williams JM, Wroblewski DA, 1988, Spatial Distribution of the Phases in Water-in-oil Emulsions. Open and Closed Microcellular Foams from Cross-linked Polystyrene. *Langmuir*, 4:656–62. DOI: 10.1021/la00081a027
 28. Robinson JL, Moglia RS, Stuebben MC, *et al.*, 2013, Achieving Interconnected Pore Architecture in Injectable PolyHIPEs for Bone Tissue Engineering. *Tissue Eng Part A*, 20:1103–12. DOI: 10.1089/ten.tea.2013.0319
 29. Knight E, Murray B, Carnachan R, *et al.*, 2011, Alvetex®: Polystyrene Scaffold Technology for Routine Three Dimensional Cell Culture. In: Haycock JW, editor. 3D Cell Culture: Methods and Protocols. Humana Press, Totowa, NJ. pp. 323–40. DOI: 10.1007/978-1-60761-984-0_20
 30. Viswanathan P, Johnson DW, Hurley C, *et al.*, 2014, 3D Surface Functionalization of Emulsion-Templated Polymeric Foams. *Macromolecules*, 47:7091–8. DOI: 10.1021/ma500968q
 31. Cameron NR, Sherrington DC, Albiston L, *et al.*, 1996, Study of the Formation of the Open-cellular Morphology of Poly(styrene/divinylbenzene) polyHIPE Materials by cryo-SEM. *Colloid Polym Sci*, 274:592–5. DOI: 10.1007/bf00655236
 32. Stevens M, Mand George J H, 2005, Exploring and Engineering the Cell Surface Interface. *Science*, 310:1135–8.
 33. Sears NA, Dhavalikar PS, Cosgriff-Hernandez EM, 2016, Emulsion Inks for 3D Printing of High Porosity Materials. *Macromol Rapid Commun*, 37:1369–74. DOI: 10.1002/marc.201600236
 34. Sears N, Dhavalikar P, Whitely M, *et al.*, 2017, Fabrication of Biomimetic Bone Grafts with Multi-material 3D Printing. *Biofabrication*, 9:025020. DOI: 10.1088/1758-5090/aa7077
 35. Susec M, Ligon SC, Stampfl J, *et al.*, 2013, Hierarchically Porous Materials from Layer-by-layer Photopolymerization of High Internal Phase Emulsions. *Macromol Rapid Commun*, 34:938–43. DOI: 10.1002/marc.201300016
 36. Johnson DW, Sherborne C, Didsbury MP, *et al.*, 2013, Macrostructuring of Emulsion-templated Porous Polymers by 3D Laser Patterning. *Adv Mater*, 25:3178–81. DOI: 10.1002/adma.201300552
 37. Lee JM, Ng WL, Yeong WY, 2019, Resolution and Shape in Bioprinting: Strategizing Towards Complex Tissue and Organ Printing. *Appl Phys Rev*, 6:011307. DOI: 10.1063/1.5053909
 38. Ng WL, Lee JM, Zhou M, *et al.*, 2020, Vat Polymerization-based Bioprinting Process, Materials, Applications and Regulatory Challenges. *Biofabrication*, 12:022001. DOI: 10.1088/1758-5090/ab6034
 39. Zhang J, Hu Q, Wang S, *et al.*, 2020, Digital Light Processing Based Three-dimensional Printing for Medical Applications. *Int J Bioprint*, 6:1–10.
 40. Thadavirul N, Pavasant P, Supaphol P, 2014, Development of Polycaprolactone Porous Scaffolds by Combining Solvent Casting, Particulate Leaching, and Polymer Leaching Techniques for Bone Tissue Engineering. *J Biomed Mater Res Part A*, 102:3379–92. DOI: 10.1002/jbm.a.35010
 41. Kim TG, Chung HJ, Park TG, 2008, Macroporous and Nanofibrous Hyaluronic Acid/collagen Hybrid Scaffold Fabricated by Concurrent Electrospinning and Deposition/leaching of Salt Particles. *Acta Biomater*, 4:1611–9. DOI: 10.1016/j.actbio.2008.06.008
 42. Sin D, Miao X, Liu G, *et al.*, 2010, Polyurethane (PU) Scaffolds Prepared by Solvent Casting/particulate Leaching (SCPL) Combined with Centrifugation. *Mater Sci Eng C*, 30:78–85. DOI: 10.1016/j.msec.2009.09.002
 43. Bencherif SA, Braschler TM, Renaud P, 2013, Advances in the Design of Macroporous Polymer Scaffolds for Potential Applications in Dentistry. *J Periodontal Implant Sci*, 43:251–61. DOI: 10.5051/jpis.2013.43.6.251
 44. Huttmacher DW, 2001, Scaffold Design and Fabrication Technologies for Engineering Tissues State of the Art and Future Perspectives. *J Biomater Sci Polym Ed*, 12:107–24.
 45. Venkatesan J, Bhatnagar I, Manivasagan P, *et al.*, 2015, Alginate Composites for Bone Tissue Engineering: A Review. *Int J Biol Macromol*, 72:269–81.
 46. Schindelin J, Arganda-Carreras I, Frise E, *et al.*, 2012, Fiji: An Open-source Platform for Biological-image Analysis. *Nat Methods*, 9:676–82. DOI: 10.1038/nmeth.2019
 47. Schneider CA, Rasband WS, Eliceiri KW, 2012, NIH Image to Image J: 25 Years of Image Analysis. *Nat Methods*, 9:671–5. DOI: 10.1038/nmeth.2089
 48. Owen R, Bahmaee H, Claeysens F, *et al.*, 2020, Comparison of the Anabolic Effects of Reported Osteogenic Compounds on Human Mesenchymal Progenitor-derived Osteoblasts. *Bioengineering (Basel)*, 7:7010012. DOI: 10.3390/bioengineering7010012
 49. Linkert M, Rueden CT, Allan C, *et al.*, 2010, Metadata Matters: Access to Image Data in the Real World. *J Cell Biol*, 189:777–82.
 50. Paljevack M, Gradišnik L, Lipovšek S, *et al.*, 2018, Multiple-Level Porous Polymer Monoliths with Interconnected Cellular

- Topology Prepared by Combining Hard Sphere and Emulsion Templating for Use in Bone Tissue Engineering. *Macromol Biosci*, 18:1700306. DOI: 10.1002/mabi.201700306
51. Hayward AS, Eissa AM, Maltman DJ, *et al.*, 2013, Galactose-functionalized PolyHIPE Scaffolds for Use in Routine Three Dimensional Culture of Mammalian Hepatocytes. *Biomacromolecules*, 14:4271–7. DOI: 10.1021/bm401145x
52. Akay G, Birch MA, Bokhari MA, 2004, Microcellular polyhipe Polymer Supports Osteoblast Growth and Bone Formation *in vitro*. *Biomaterials*, 25:3991–4000. DOI: 10.1016/j.biomaterials.2003.10.086
53. Workman VL, Dunnett SB, Kille P, *et al.*, 2008, On-Chip Alginate Microencapsulation of Functional Cells. *Macromol Rapid Commun*, 29:165–70. DOI: 10.1002/marc.200700641
54. Beck GR Jr., Zerler B, Moran E, 2001, Gene Array Analysis of Osteoblast Differentiation. *Cell Growth Differ*, 12:61–83.